Article:
(2017) Non-Local Effects on Pedestal Kinetic Ballooning Mode Stability. Plasma Physics and Controlled Fusion. 064001. ISSN 1361-6587

https://doi.org/10.1088/1361-6587/aa66ab

Non-Local Effects on Pedestal Kinetic Ballooning Mode Stability

S. Saarelma[1]

J. Martin-Collar[2]

D. Dickinson[3]

B.F. McMillan[2]

C.M. Roach[1]

MAST team[1]

The JET Contributors†

EUROfusion Consortium JET Culham Science Centre, Abingdon, OX14 3DB, UK
[1] CCFE, Culham Science Centre, Abingdon, Oxon OX14 3DB, UK
[2] Centre for Fusion, Space and Astrophysics, Warwick University, Coventry CV4 7AL, UK
[3] York Plasma Institute, Dept. of Physics, University of York, York, YO10 5DD, UK
samuli.saarelma@ukaea.uk

Abstract

The H-mode pedestal height plays an important role in determining the global confinement of the tokamak plasma. In type I ELMy H-mode the ultimate limit for the pedestal pressure at constant width is set by the ideal MHD peeling-ballooning modes that are thought to be the trigger for the ELMs. However, the peeling-ballooning mode criterion does not uniquely determine the pedestal. Increasing the width of the pedestal, the marginally peeling-ballooning stable pedestal height increases as well. The second criterion for the pedestal is set by the transport processes in the pedestal that limit the gradient between the ELMs.

One candidate for driving this transport is the kinetic ballooning mode (KBM) that is driven by the pressure gradient [1]. The KBM growth rate increases very rapidly after the critical pressure gradient is exceeded leading to very stiff profiles

† See the Appendix of F. Romanelli et al., Proceedings of the 25th IAEA Fusion Energy Conference 2014, St Petersburg, Russia

with the pressure gradient clamped near to the stability limit. In the local linear gyrokinetic analysis of experimental MAST and JET plasmas we have found that, like the n=∞ ideal MHD ballooning modes, the KBMs can access locally so called second stability if the magnetic shear becomes low enough [2, 3]. However, in the pedestal region the local assumption that the equilibrium can be considered radially constant for the investigated modes is no longer justified. In this paper we revisit the KBM analysis using a global code ORB5 to investigate whether second stability access exists for KBMs.

We find that counter to the local analysis, the global KBM stability is not sensitive to the magnetic shear in the pedestal region. At sufficiently high β (but still below the ideal peeling-ballooning limit) the pedestal region becomes KBM unstable regardless of the amount of bootstrap current assumed in the equilibrium reconstruction. However, just as in local analysis, the mode is stabilised by reducing the pressure gradient. This suggests that KBMs can regulate the pedestal pressure gradient during the ELM cycle even when local analysis finds them stable due to high bootstrap current.

PACS numbers: 52.55.Fa

Submitted to: *Plasma Physics and Controlled Fusion*

1. Introduction

The energy transport in tokamak core plasmas is dominated by turbulence which restricts the normalised temperature gradient $\nabla T/T$ near the marginal stability limit as the turbulent transport increases rapidly when the gradient exceeds the critical value [4]. This stiff transport dictates that increasing core heating will not be very effective at increasing the core temperature, but will just increase the turbulent heat flux. Instead to increase the core temperature the edge temperature should be as high as possible. In the high confinement mode or H-mode good global plasma confinement is achieved by creating a so-called pedestal in temperature and density profiles near the edge of the plasma.

The pedestal region is characterised by a steep pressure gradient that is a source of intermittent instabilities called Edge Localised Modes or ELMs that lead to a relaxation of the pedestal gradient and expulsion of heat and particles from the edge plasma. It has been observed in several devices that the edge plasma is close to the peeling-ballooning mode (PBM) stability limit just prior to an ELM crash [1]. Thus, the peeling-ballooning modes that are driven by the edge pressure gradient and the strong bootstrap current peak in the gradient region, limit the maximum achievable pedestal height for a given width of the pedestal. However, changing the width of the pedestal changes also the peeling-ballooning mode limited height of the pedestal as the peeling-ballooning modes mainly limit the gradient with a weak dependence on the width. Consequently, the peeling-ballooning mode stability limit alone is not sufficient to predict the pedestal height.

In order to fully predict the pedestal of a given plasma configuration, another constraint for the width (or gradient) is needed. Experimentally, several devices (JT-60U [5], MAST [6], DIII-D [7]) have observed that the dependency of $\Delta \sim \sqrt{\beta_{p,ped}}$, where Δ is the width of the pedestal and $\beta_{p,ped}$ is poloidal β evaluated at the pedestal top. However, this dependency does not seem to be universal, as a linear dependency between the width and the height ($\Delta \sim \beta_{p,ped}$) was observed in NSTX [8]. Also pedestal widening without a change in height has been observed with increased gas fuelling in JET with the Beryllium-Tungsten wall [9]. Therefore, relying on the empirical $\Delta \sim \sqrt{\beta_{p,ped}}$ scaling without understanding the physical basis of the scaling can lead to wrong answers especially if it is used for future devices operating outside the parameters used in current experiments.

A candidate for the physical explanation of the scaling used in the most developed pedestal prediction model today, EPED [10, 11], is that the pedestal gradient is constrained by the kinetic ballooning modes (KBM) between ELMs leading to the widening of the pedestal with fixed gradient until the peeling-ballooning mode limit is reached. The KBM is a long wavelength ($k_\perp \rho_i < 1$) mode propagating in the ion diamagnetic direction and is closely related to the ideal MHD ballooning mode and in local approximation it is assumed to have a so-called second stability region at low magnetic shear [12]. A mode showing characteristics of KBMs has been observed in NSTX between ELMs with the pedestal being close to the $n = \infty$ ideal MHD ballooning mode limit [13]. Also DIII-D [14] and MAST [15] have observed modes that agree with some of the characteristics of KBMs.

Local gyrokinetic calculations have identified KBMs in the pedestal region of MAST [2, 16], DIII-D [17] and JET [3]. In all of these analyses the linear KBM onset was found to be close to the ideal MHD $n = \infty$ ballooning mode limit. However all of the analyses found only weak or no KBM drive in the steepest gradient region, where

the current density is the highest and the magnetic shear the lowest. Especially in JET with the lowest collisionality and the highest edge current density the magnetic shear becomes so low that the ideal MHD $n = \infty$ modes access the second stable region. In local gyrokinetic analysis this is seen as complete stabilisation of the KBMs. These local results cast doubt on the possibility that KBMs may indeed limit the pedestal pressure gradient.

However, the local gyrokinetic analysis assumes that the gradient length scales are much larger than the studied mode structure. Whilst this assumption is usually valid in the core and even at the pedestal top, in the pedestal region the gradients can be so steep that the assumption is no longer valid. The mode can cover a large fraction of the pedestal leading to a large variation of equilibrium profiles in the simulated region. For instance, in MAST pedestal with $\Delta \approx 5\rho_i$ the KBM has the peak growth rate at $k_\perp \rho_i \approx 0.2$, where $k_\perp$ is the perpendicular wave number and ρ_i is the ion Larmor radius [2]. This necessitates taking into account non-local effects on the instabilities. For KBMs two in particular are important. On one hand, since the pressure gradient varies strongly within the pedestal, the drive of the KBM with a finite width is smaller than the drive of the infinitesimal $n = \infty$ ballooning mode assumed in the ideal MHD analysis. On the other hand, while the parts of the pedestal where shear is very low allow access the second stable region for local $n = \infty$ ballooning modes, a mode extending across the pedestal may not be able to access the second stability [18].

In this paper we investigate the non-local effects in pedestal conditions using a global gyrokinetic code. As a basis of the analysis we use equilibria and profiles based on the earlier JET and MAST local analyses [2, 3]. The main emphasis in the analysis is in the behaviour of the second stability access, which we study by comparing the equilibria created with and without the bootstrap current peak in the pedestal. The equilibria created with the bootstrap current have access to the second stable region for $n = \infty$ ballooning modes and KBMs, while the equilibria without the bootstrap current are in the unstable region.

2. Local Gyrokinetic Analysis

To connect with previous work, we use in this analysis equilibria that are based on previous analyses of MAST[2] and JET[3] pedestals. In both cases, KBMs were identified in the pedestal with the unstable region matching very well to the ideal MHD $n = \infty$ ballooning unstable region. In JET, it was found that the local KBM unstable region depended very strongly on the magnetic shear giving the centre of the pedestal region access to so called second stability if the bootstrap current was high enough to flatten or even reverse the q-profile in the pedestal. In the original MAST analysis, no second stability access was observed either in gyrokinetic KBM analysis or in the ideal MHD $n = \infty$ ballooning stability, but this was due to high collisionality of the studied plasma [2, 16]. Later analyses[19, 20] of lower collisionality MAST pedestals found that KBMs and $n = \infty$ ideal MHD ballooning modes had local access to second stability as was found in JET. The conclusion in both cases was that in a local gyrokinetic analysis a pedestal with sufficiently low bootstrap current was KBM unstable, but the increase of bootstrap current stabilised the KBMs in the pedestal centre leaving only the bottom of the pedestal close to the KBM stability limit.

It was necessary to modify the equilibria of previous analyses, in order to analyse these phenomena with a global gyrokinetic code. The main reason is that in the global analysis, the treatment of the computational domain edge can affect the results if the

growing modes that are too close it. Therefore, we modify the equilibria by shifting the profiles inwards thus creating a region with flat density and temperature profiles near the plasma edge. This modification produces a buffer region with flat profiles for the global analysis. Before going to the global case, we test that the previous local result is qualitatively reproduced with the new equilibria.

2.1. Modified JET Discharge #79503

The JET equilibrium is based on the JET discharge #79503, which has plasma current of 2.5MA, toroidal field of 2.65T and upper triangularity of 0.41. The experiment is described more in detail in [21]. In this paper, we shift the temperature and density profiles inwards 10% in normalised poloidal flux in order to create a buffer zone between the pedestal and the plasma edge. As in the earlier analysis [3] we make the plasma shape up-down symmetric by cloning the shape above the midplane to be the plasma shape also below the midplane. To maximise the effect that we are trying to study, namely the effect of flattened shear on the KBM stability, we increase the bootstrap current driven by the input density and temperature profiles by 100%. We also create an equilibrium where the bootstrap current is set to zero. The q profile and the shifted and pressure profile of the resulting equilibria as well as the original measured JET pressure profile are shown in Fig 1. The q-profile is locally flattened in the pedestal region with the bootstrap current.

While the resulting equilibria are somewhat different from the experimental equilibria and thus, the results presented here are not considered to quantitatively apply to an experimental JET plasma, the qualitative properties should not have been changed significantly. We test this by repeating the local analysis as was performed for the original experimental case, comparing the local ideal $n = \infty$ ballooning mode stability to the KBM stability calculated using the local electromagnetic GS2 code [22]. GS2 is run in the linear mode without collisions. While GS2 can find other unstable modes in the pedestal, in this analysis we only consider modes that can be identified as KBMs, i.e. they have long wavelength ($k_\perp \rho_i < 0.3$), propagate in the ion diamagnetic direction and their growth rate is sensitive to the variation of β. The local ideal MHD $n = \infty$ ballooning stability is calculated together with the equilibrium reconstruction using the equilibrium code HELENA [23].

As can be seen in Fig.2 the unstable region for $n = \infty$ ballooning modes agrees very well with the KBM unstable region. The KBM growth rates are normalised to v_{Ti}/a, where v_{Ti} is the ion thermal velocity and a is the minor radius. Only the equilibrium without the bootstrap current finds KBMs locally unstable in the steep pedestal region. This is qualitatively exactly the same stability picture as was found for the original experimental equilibrium without the radial shift. As mentioned above, the collisions were ignored to be better compatible with the global analysis. In any case their effect on the KBM stability was confirmed to be small when we repeated the local analysis with collisions.

We perform a local β scan for the case without bootstrap current at the flux surface with the steepest pressure gradient ($\psi = 0.88$) to determine how deep in the KBM unstable region the pedestal is. In the scan the parameter β only influences the strength of the magnetic perturbation, and the scan is inconsistent in the sense that the local equilibrium and density and temperature profiles are unchanged. As can be seen in Fig. 3, β has to be lowered to about half of the value in the original equilibrium to stabilise the KBMs. Figure 3 also shows the growth rate spectrum that

we can compare with global analysis.

We perform similar β-scan to the equilibrium with bootstrap current. In this case, the KBMs were stable even when β was increased by a factor of 4. This is clearly a sign of an access to second stability.

2.2. Modified MAST Discharge #24763

For the same reasons as with the JET equilibrium, we modify the equilibrium from MAST discharge #24763 using the profiles in the last 20% of the ELM cycle by shifting the profiles inwards by 4% in normalised poloidal flux. This discharge has $I_p = 850kA$, $B_t = 0.585T$ at the magnetic axis, $P_{NBI} = 3.4$ MW and triangularity of 0.47. Again we create two equilibria, one without bootstrap current and one with 100% enhanced bootstrap current. As in the JET case the bootstrap current is enhanced to increase the access to second stability in the local analysis and decreased to close the access completely. The gradients of the density and temperature profiles in the core have also been reduced to limit the instability drive in the core region, which is necessary in the global analysis to avoid core modes dominating the pedestal modes. This has a small effect on the local pedestal stability as the reduced Shafranov-shift destabilises the pedestal ballooning modes. The equilibrium q and pressure profiles are shown in Fig 4.

The local gyrokinetic growth rates of KBMs in the pedestal region using GS2 and the local ideal MHD $n = \infty$ ballooning mode stability are shown in Fig. 5. As in the JET case, the unstable regions agree very well in the MHD and gyrokinetic analyses. However, in this case, even the case without bootstrap current has a large stable region in the steepest part of the pedestal pressure gradient. Only the region close to the bottom of the pedestal ($\psi_N = 0.95 - 0.96$), becomes unstable to both $n = \infty$ and KBM in the no bootstrap current case. The width of the unstable region in the no bootstrap case is about three ρ_i at the midplane. Figure 6 shows the growth rate spectrum of the KBMs at the most unstable location, $\psi_N = 0.955$ for the no bootstrap case. For the most unstable modes$n = 7$ corresponding $k_\theta \rho_i \approx 0.1$, which means that the mode wavelength is much larger than the radial width of the unstable region. Poloidally the unstable KBMs peak at the low field side midplane. Even small variation of θ or the poloidal localisation of the mode from the midplane leads to the stabilisation of the mode.

Similar to JET, we perform a β scan for the MAST equilibrium without the bootstrap current for the flux surface that was found KBM unstable ($\psi_N = 0.955$). As can be seen in Fig. 7 we find the β limit for KBMs to be slightly lower than the ideal MHD $n = \infty$ ballooning mode limit for the case without bootstrap current. On the other hand, the equilibrium with bootstrap current is much more stable for KBMs as no stability limit was found within the investigated β range suggesting that the plasma is accessing the 2^{nd} stability at this location.

3. Global Gyrokinetic Analysis

The local ρ_i/a at the top of the pedestal is 1/600 for the JET and 1/180 for the MAST equilibrium. This would suggest that the local treatment is sufficient. However, a more relevant measure for pedestal equilibrium variation, ρ_i/Δ, where Δ is the pedestal width is 1/15 for the JET and 1/4 for the MAST equilibrium. Therefore, we expect the non-local equilibrium effects to modify the local gyrokinetic result.

The linear global gyrokinetic analysis of the pedestals is conducted using the ORB5 code [24]. ORB5 is a global electromagnetic particle-in-cell (PIC) code. The formulation of the electromagnetic equations solved by ORB5 is derived in [25]. ORB5 can include particle collisions, but since we found in the local analysis that collisions had little effect on the KBMs, all the global runs are done assuming collisionless plasma. We simulate the region of $0.64 < \psi_N < 1$.

The inner boundary is far from the pedestal and requires no special treatment, but in the outer boundary we use shielding to suppress the linear drive in a buffer zone to avoid the boundary condition impacting on the pedestal region. The shielding is done by modifying the density used to define the background ion polarisation response by:

$$n(s) = n(s)1 + \kappa_{sh} C \sinh\left(\frac{(s - s_{min})/(s_{max} - s_{min})}{w_{sh}}\right), \quad (1)$$

$$C = \frac{1}{\sinh\left(\frac{1}{w_{sh}}\right)}, \quad (2)$$

where s_{min} and s_{max} are the minimum and maximum values of s in the simulation domain, κ_{sh} is the amplitude of the shielding and w_{sh} is the width of the shielding. The shielding parameters have little effect on the results as long as the width of the shielding does not reach the steep gradient region.

The grid resolution that we use is $N_s = 300$, $N_\chi = 1024$, $N_\phi = 256$, where s is the radial, χ the poloidal and ϕ the toroidal direction. To test the required marker number, we perform a scan using 4, 8 and 16 million markers. The field energy plots for the three cases are shown in Fig 8. It can be seen that 8 million markers is sufficient to resolve the growth rate. The results presented here are done using 8 million markers.

To save computational resources the global analyses here are done using the mass ratio m_D/m_e of 200, which is smaller than the real mass ratio of 3672. However, we found in the local analysis that the mass ratio makes little ($< 20\%$) difference on the growth rate.

3.1. Modified JET Discharge #79503

We first conduct a toroidal mode number scan to compare with the spectrum found in the local analysis. Figure 9 a) shows the growth rates as a function of toroidal mode number for both equilibria with and without bootstrap current. The peak of the spectrum ($n \approx 40$) is shifted to higher mode numbers than what was found in the local analysis for the equilibrium without the bootstrap current, Fig. 3 ($n \approx 20$). Furthermore, the global analysis shows practically no difference between the cases with and without bootstrap current, while the case with bootstrap current was completely stable in the local analysis. The other point to note is that the growth rates of global KBMs are significantly higher than found in the local analysis.

Similar to the local analysis we conduct a β scan using the global code. Unlike in the local scan, here we recalculate the equilibrium for each value of β as the equilibrium changes can affect the global result. In the equilibrium reconstruction the density gradient is increased along with β. Also the bootstrap current is calculated self-consistently for each equilibrium. We find that the global β limit for equilibria with and without bootstrap current are higher than the local limit for the equilibrium without the bootstrap current, but lower than the local limit for the equilibrium with the bootstrap current Fig 3.

3.2. Modified MAST Discharge #24763

The global analysis is repeated for the MAST discharge. The spectrum and the β dependence of the KBMs in the pedestal are shown in Fig. 10. Again the peak of the spectrum ($n \approx 20$) is shifted to higher n compared to the local result ($n \approx 7$) without bootstrap current, and the growth rates are higher. The bootstrap current case has the same spectrum as the no bootstrap current which is different from the local result that is stable for pedestal KBMs. The global β-scan shows that as in the JET pedestal there is no difference in the stability limit between the cases with and without bootstrap current.

The global KBM stability limit with and without the bootstrap current is close to the $n = \infty$ ideal ballooning and local KBM limit of the equilibrium without the bootstrap current, shown in Fig. 7. So, while the global effects degrade the stability if the pedestal locally has access to 2^{nd} stability, they do not seem to affect the stability of the case that does not have the 2^{nd} stability access.

It should also be noted here that the radial extent of the KBMs covers the entire pedestal. We purposefully shifted the pedestal inwards to avoid effects from the simulation domain edge. It is, however, possible that the real plasma separatrix has an impact on the KBMs, and a realistic treatment of the edge and the surrounding scrape-off-layer is required to quantitatively calculate the stability limits of the KBMs. However, that is beyond the scope of this paper as we are here investigating the non-local effects on the 2^{nd} stability access of the KBMs. The boundary effects are likely to be similar for both equilibria with and without bootstrap current.

4. Conclusions

The access to 2^{nd} stability for KBMs present in the local gyrokinetic and ideal $n = \infty$ MHD analysis in the pedestal region with high bootstrap current was not found in the global electromagnetic gyrokinetic simulations presented in this paper for modified JET and MAST equilibria. For the MAST pedestal the global β limit for the KBMs is found to be close to the local β limit found for the equilibrium reconstructed without the bootstrap current. The inclusion of bootstrap current into the equilibrium gives access to the 2^{nd} stability for KBMs in the local analysis but has no effect on the global KBM stability limits. The global KBM β limit for the JET pedestal is insensitive to the bootstrap current, but in this case it is higher than the local limit for the equilibrium without the bootstrap current in the MAST and JET equilibria that we have studied.

The global spectrum of linear growth rates shifts to higher mode numbers compared with the local result. This is due to the finite radial width of the KBMs. The drive to the KBMs is maximised in the steep pressure gradient region of the pedestal. The low-n modes with wider radial width extend more outside of this region, which lowers the drive to the KBMs. The narrower high-n modes are less affected by this reduction in linear drive but are still sufficiently extended that they can not access second stability.

The insensitivity of the global KBM stability to the details of the q-profile agrees with the global analysis by Wan et al. [26] for the intermediate-n KBMs that were not affected by the change in q-profile. All the equilibria used in this paper were stable for low-n peeling-ballooning modes that were found to be stabilised by the q-profile flattening in [26]. Low-n MHD modes tend to be peeling-ballooning modes (PBM) in the pedestal, and these are not captured in the lowest order gyrokinetic

model used in codes like GS2 and ORB5. This is why we would not expect agreement with the fluid limit at low n in conditions where PBMs dominate. The point is that equilibrium parallel current density gradient drive that is necessary to describe PBMs is missing from the local non-shifted Maxwellian background distribution function f_0 used here [24]. In [26], where the gyrokinetic model must have been extended somehow to include the current gradient drive, the stabilising effect of flattening q-profile was found for low-n modes (identified as kinetic peeling-ballooning mode, or peeling-ballooning mode in [27]). However the KBMs with n=20-60 in [26] are affected only slightly and actually destabilised by the q-profile flattening. We believe that the global gyrokinetic modes that are presented in Figs. 9 a) and 10 a) are the same KBMs that were found in [26] (KBM torodial mode numbers for conventional aspect ratio tokamak DIII-D analysis in [26] are the same as those for JET in this paper. They are slightly lower for the tight aspect ratio tokamak MAST).

Furthermore, the equilibria that were the basis of this paper [2, 3] were not ideal MHD unstable to low-n PBM. The MHD stability analysis of the modified equilibria used in this paper also found no unstable low-n ($n < 10$) ideal MHD modes. In the global gyrokinetic analysis we did not find low-n modes either. So, in that sense the global gyrokinetic analysis and MHD analysis of low-n modes agree with each other. Further work with equilibria unstable to low-n peeling modes would be required to study the stabilising effect found in [26].

Since the global result indicates that the 2^{nd} stability access for KBMs may not exist when the non-local effects are taken into account, the predictive pedestal models constructed using local stability criteria of KBMs to constrain the pedestal gradients should not use the equilibria with full self-consistent bootstrap current. Instead the global stability limit for an equilibrium with the bootstrap current can be more accurately approximated by the local result of an equilibrium that has artificially suppressed bootstrap current in the pedestal.

Acknowledgement

This work has been carried out within the framework of the EUROfusion Consortium and has received funding from the Euratom research and training programme 2014-2018 under grant agreement No 633053 and from the RCUK Energy Programme [grant number EP/I501045]. The work is part of the EUROfusion Enabling Research project CfP-WP15-ENR-01/CCFE-03. The views and opinions expressed herein do not necessarily reflect those of the European Commission. This computational work was carried out using the HELIOS supercomputer systems at Computational Simulation Centre of International Fusion Energy Research Centre (IFERC-CSC), Aomori, Japan, under the Broader Approach collaboration between Euratom and Japan, implemented by Fusion for Energy and QST. Further computational resources were provided by the Plasma HEC Consortium (EP/L000237/1)

References

[1] P.B. Snyder et al., Nucl. Fusion **49** (2009) 085035.
[2] D. Dickinson et al., Plasma Phys. Control. Fusion **53** (2011) 115010.
[3] S. Saarelma et al., Nucl. Fusion **53** (2013) 123012.
[4] F. Ryter et al., Plasma Phys. Control. Fusion **43** (2001) A323.
[5] H. Urano et al., Nucl. Fusion **48** (2008) 045008.
[6] A. Kirk et al., Plasma Phys. Control. Fusion **51** (2009) 065016.

[7] R.J. Groebner et al., Nucl. Fusion **49** (2009) 085037.
[8] A. Diallo et al, Nucl. Fusion **53**, 093026 (2013).
[9] M. Leyland et al, Nucl. Fusion **55**, 013019 (2015).
[10] P.B. Snyder et al., Phys. Plasmas **16** (2009) 056118.
[11] P.B. Snyder et al., Nucl. Fusion **51** (2011) 103016.
[12] B.-G. Hong et al., Phys. Fluids B 1, **1589** (1989).
[13] A. Diallo et al., Phys. Rev. Lett. **112** (2014) 115001.
[14] Z. Yan et al., Phys. Plasmas **18** (2011) 056117
[15] A. Kirk et al., Nucl. Fusion **54** (2014) 114012.
[16] D. Dickinson et al., Phys. Rev. Lett. **108** (2012) 135002.
[17] E. Wang et al., Nucl. Fusion **52** (2012) 103015.
[18] H. R. Wilson and R. L. Miller, Phys. Plasmas **6** (1999) 873.
[19] S. Saarelma et al., 39^{th} EPS Conference on Plasma Physics, Stockholm, Sweden (2012) O4.111
[20] C.M. Roach et al. Proceedings of the 24th IAEA Fusion Energy Conference 2012, San Diego, USA, TH/5-1.
[21] M.J. Leyland et al. Nucl. Fusion **53** (2013) 083028
[22] Kotschenreuther M., et al., Comput. Phys. Commun **88** (1995) 128
[23] Huysmans G.T.A., Goedbloed J.P., Kerner W.O.K., Computational Physics (Proc. Int. Conf. Amsterdam, 1991),World Scientific Publishing, Singapore (1991) 371
[24] S. Jolliet et al, Comput. Phys. Commun. **177** (2007) 409
[25] A. Bottino et al., Plasma Phys. Control. Fusion **53** (2011) 124027
[26] W. Wan et al. Phys. Rev Lett. **109** (2012) 185004
[27] P. Zhu el al., Phys. Plasma **19** (2012) 032503

Figure captions

Figure 1. The profiles of q (left) and pressure (right) of the modified JET equilibria. The crosses show the actual JET pressure data measured by the Thomson scattering system and the solid line shows the modified profile used in the analysis.

Figure 2. The ideal MHD $n = \infty$ ballooning stability for the modified JET equilibria with and without bootstrap current (left). The black line shows the equilibrium pressure gradient and the coloured lines show the stability boundaries. The local growth rate of the KBMs in the pedestal region for the same equilibria (right)

Figure 3. The local growth rate of the KBMs as a function of toroidal mode number n for the modified JET equilibrium at $\psi_N = 0.88$ without bootstrap current with varying β. The value $\beta = 0.21\%$ corresponds to the equilibrium value. The $n = \infty$ ideal ballooning limit on this flux surface is at $\beta = 0.16\%$.

Figure 4. The profiles of q (left) and pressure (right) of the modified MAST equilibria. Also the original pressure profile is shown.

Figure 5. The ideal MHD $n = \infty$ ballooning stability for the modified JET equilibria with and without bootstrap current (left). The black line shows the equilibrium pressure gradient and the coloured lines show the stability boundaries. The local growth rate of the KBMs in the pedestal region for the same equilibria (right).

Figure 6. The growth rate as a funtion of toroidal mode number of the modified MAST equilibrium without bootstrap current at $\psi_N = 0.955$

Figure 7. The maximum local growth rate of the KBMs as a function of β for both with and without bootstrap current at this location. Also the $n = \infty$ ballooning limit (blue dashed) is shown.

Figure 8. The energy in the n=10 linear simulation for the MAST equilibrium as a function of time for 4, 8 and 16 million markers.

.

Figure 9. The growth rate as a function of n (a) and the n=30 growth rate as a function of β (b) in global analysis with ORB5 for JET equilibria with (red) and without (blue) bootstrap current. The normalising v_{ti} and β are evaluated at $\psi_N = 0.865$. The equilibrium β is 0.35%

Figure 10. The growth rate as a function of n for $\beta = 0.12\%$ (a) and the n=10 mode growth rate as a function of β (b) in global analysis with ORB5 for MAST equilibria with (red) and without (blue) bootstrap current. The normalising v_{ti} and β are evaluated at $\psi_N = 0.955$. The equilibrium β is 0.25%

Figures

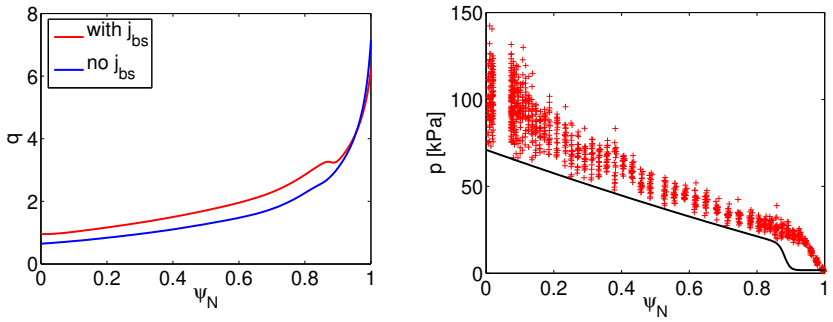

Figure 1. The profiles of q (left) and pressure (right) of the modified JET equilibria. The crosses show the actual JET pressure data measured by the Thomson scattering system and the solid line shows the modified profile used in the analysis.

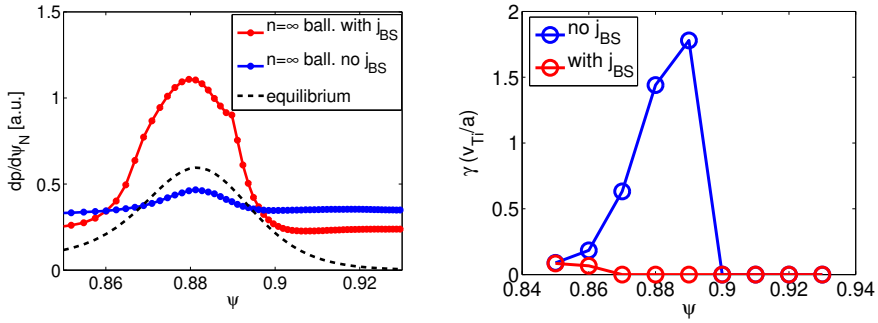

Figure 2. The ideal MHD $n = \infty$ ballooning stability for the modified JET equilibria with and without bootstrap current (left). The black line shows the equilibrium pressure gradient and the coloured lines show the stability boundaries. The local growth rate of the KBMs in the pedestal region for the same equilibria (right)

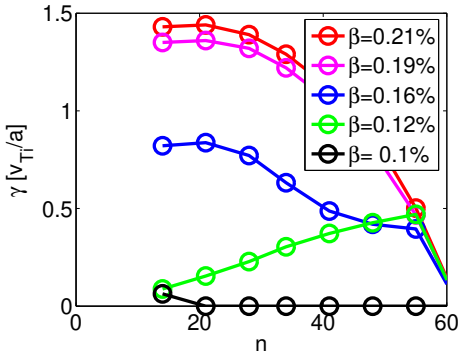

Figure 3. The local growth rate of the KBMs as a function of toroidal mode number n for the modified JET equilibrium at $\psi_N = 0.88$ without bootstrap current with varying β. The value $\beta = 0.21\%$ corresponds to the equilibrium value. The $n = \infty$ ideal ballooning limit on this flux surface is at $\beta = 0.16\%$.

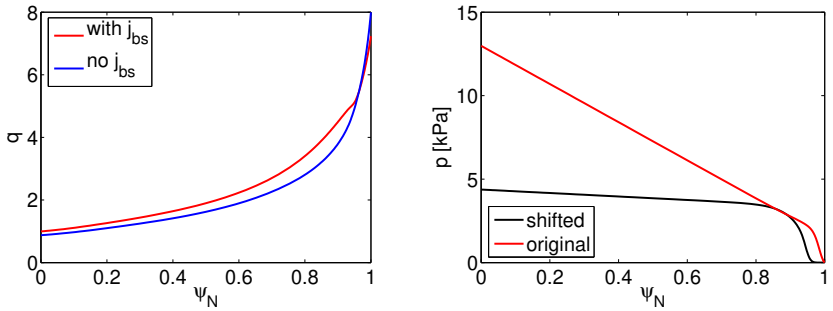

Figure 4. The profiles of q (left) and pressure (right) of the modified MAST equilibria. Also the original pressure profile is shown.

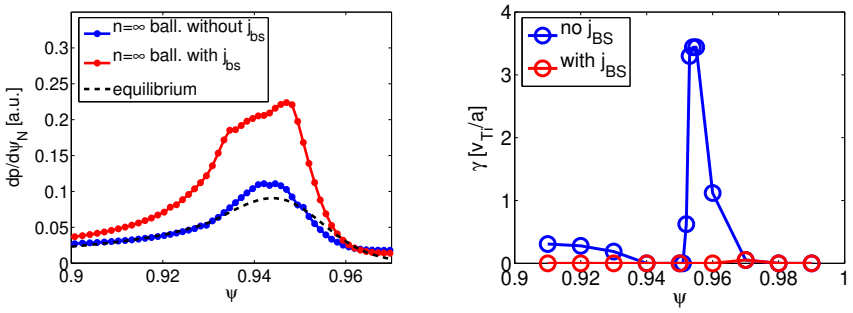

Figure 5. The ideal MHD $n = \infty$ ballooning stability for the modified JET equilibria with and without bootstrap current (left). The black line shows the equilibrium pressure gradient and the coloured lines show the stability boundaries. The local growth rate of the KBMs in the pedestal region for the same equilibria (right).

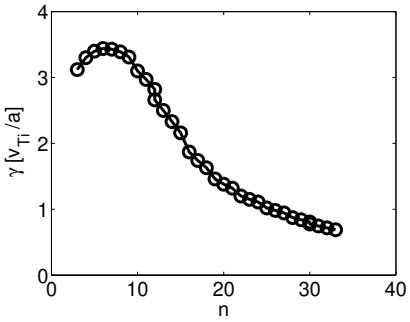

Figure 6. The growth rate as a funtion of toroidal mode number of the modified MAST equilibrium without bootstrap current at $\psi_N = 0.955$

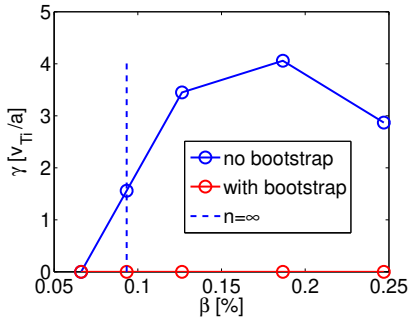

Figure 7. The maximum local growth rate of the KBMs as a function of β for both with and without bootstrap current at this location. Also the $n = \infty$ ballooning limit (blue dashed) is shown.

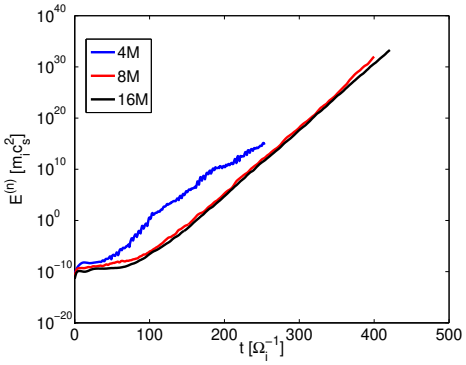

Figure 8. The energy in the n=10 linear simulation for the MAST equilibrium as a function of time for 4, 8 and 16 million markers.

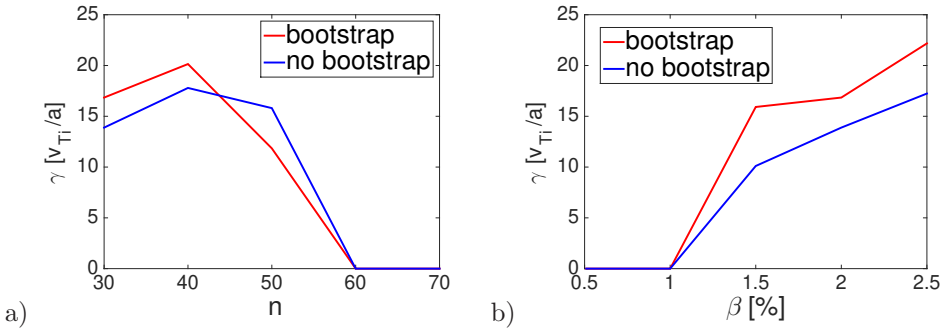

a) b)

Figure 9. The growth rate as a function of n (a) and the n=30 growth rate as a function of β (b) in global analysis with ORB5 for JET equilibria with (red) and without (blue) bootstrap current. The normalising v_{ti} and β are evaluated at $\psi_N = 0.865$. The equilibrium β is 0.35%

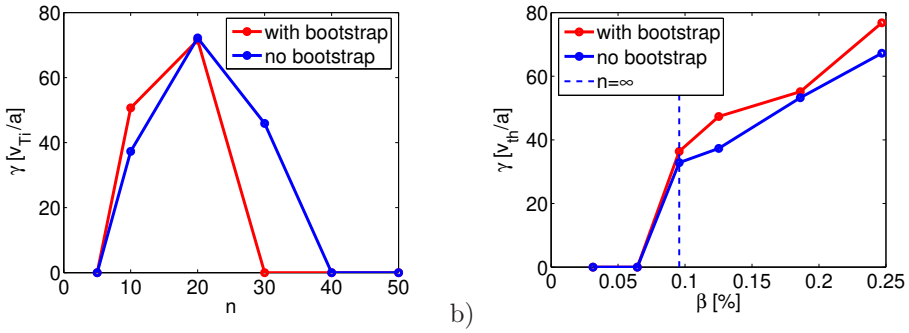

a) b)

Figure 10. The growth rate as a function of n for $\beta = 0.12\%$ (a) and the n=10 mode growth rate as a function of β (b) in global analysis with ORB5 for MAST equilibria with (red) and without (blue) bootstrap current. The normalising v_{ti} and β are evaluated at $\psi_N = 0.955$. The equilibrium β is 0.25%